Explanations for the observed increase in fast electron penetration in laser shock compressed materials

D. Batani,[1] J. R. Davies,[2] A. Bernardinello,[1] F. Pisani,[1] M. Koenig,[3] T. A. Hall,[4] S. Ellwi,[4] P. Norreys,[5] S. Rose,[5] A. Djaoui,[5] and D. Neely[5]

[1]*Dipartimento di Fisica ''G. Occhialini,'' Università degli Studi di Milano - Bicocca and INFM, Via Emanueli 15, 20126 Milano, Italy*

[2]*Instituto Superior Técnico, GoLP, 1049-001 Lisboa, Portugal*

[3]*LULI, UMR 7605, CNRS-CEA-X-Paris VI, Ecole Polytechnique, 91128 Palaiseau, France*

[4]*Department of Physics, University of Essex, Colchester CO4 3SQ, United Kingdom*

[5]*Rutherford Appleton Laboratory, Chilton, Didcot, Oxon OX11 0QX, United Kingdom*

(Received 18 October 1999)

We analyze recent experimental results on the increase of fast electron penetration in shock compressed plastic [Phys. Rev. Lett. **81**, 1003 (1998)]. It is explained by a combination of stopping power and electric field effects, which appear to be important even at laser intensities as low as 10^{16} W cm^{-2}. An important conclusion is that fast electron induced heating must be taken into account, changing the properties of the material in which the fast electrons propagate. In insulators this leads to a rapid insulator to conductor phase transition.

PACS number(s): 52.50.−b, 52.40.−w, 52.35.−g

I. INTRODUCTION

In inertial confinement fusion (ICF) research a new approach, the so called ''fast ignitor,'' was devised [1,2] to achieve the goal of ignition. Crucial to the success of this approach is the study of its last phase: the propagation of fast electrons and their energy deposition in the compressed pellet. The problem has, until recently, only been studied in numerical and theoretical works [3], and no experimental results were available. Recently, the first experimental measurement on the propagation of laser generated fast electrons in compressed materials was performed at the Rutherford Laboratory [4,5]. The VULCAN laser system [6] was used both to shock compress plane plastic targets (CH_2), using 2-ns beams, and to generate fast electrons on the other side of the targets, using the chirped pulse amplified (CPA) beam. This experiment showed a much increased penetration of fast electrons in the compressed plastic (see Fig. 1). The objective of this paper is a theoretical interpretation of these results.

The two compression beams were frequency doubled to 0.503 μm, and yielded about 50 J each on target in 2-ns duration pulses. The use of random phase plates [7] for optical smoothing led to focal spot diameters of about 250 μm, giving a total intensity on target $\leqslant 10^{14}$ W cm^{-2}. Figure 2 shows the results of a simulation of the shock compression phase, performed with the hydrodynamic code MULTI [8], which gives the density and temperature profiles in the target as a function of time. The experimentally measured shock velocity D is in very good agreement with that obtained from MULTI using the SESAME [9] equations of state for plastics. It gives a compression factor $\rho/\rho_0 \approx 3.2$, a temperature of ≈ 6 eV and a pressure of ≈ 8 Mbar for $D \approx 32$ km s^{-1}. The corresponding value of ionization is $Z^* \approx 1.7$. The correlation and degeneracy parameters of the shock compressed material were calculated to be $\Gamma \approx 6.1$ and $E_F/T \approx 3.7$, respectively (where E_F is the Fermi energy, calculated including the first thermal correction [10]). This indicates that our plasma is both correlated and degenerate.

The CPA beam delivers 10–30 J in 1–3 ps. The focal spot diameter ranged from 100 to 180 μm, giving intensities of $(1-6)\times 10^{16}$ W cm^{-2}. To maximize the fast electron generation, a 30° angle of incidence and P polarization were used [11,12]. The timing between the CPA and ns beams was chosen so that ≈ 8 μm of uncompressed material was present when the CPA beam was fired. This ensured that the conditions of fast electron generation were identical in both the cold and shock-compressed cases. The intensity was kept deliberately low so that the expected range of the fast electrons would approximately match the target thickness, which was limited by the thickness that could be uniformly shock compressed.

The propagation of the electrons through the target was studied using $K\alpha$ spectroscopy with a chlorinate plastic (PVCD) fluor layer ($\rho = 1.64$ g/cm^3), producing $K\alpha$ emission from chlorine at 2622 eV. A 13.5 μm of PVCD fluor

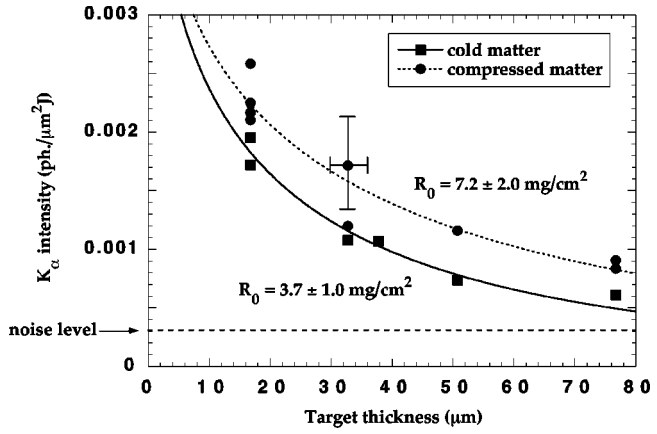

FIG. 1. $K\alpha$ experimental yield and penetration depth for cold and compressed matter as a function of target thickness in μm (taken as the midpoint of the fluor layer). Also shown are the typical error bars, the typical noise level, and the interpolation using Harrach and Kidder's model.

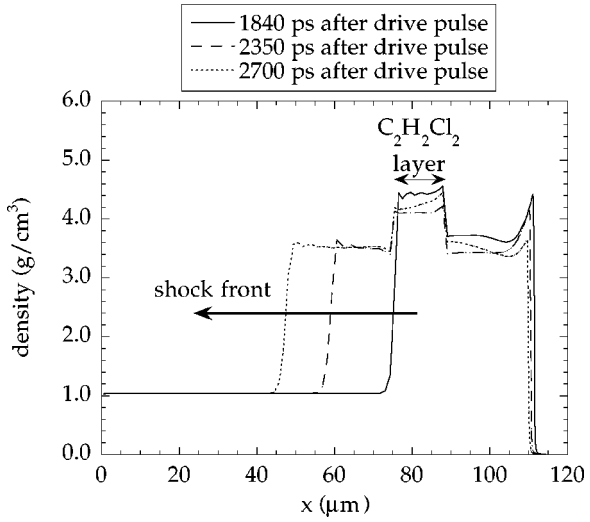

FIG. 2. Density profiles obtained from numerical simulations performed with the hydrodynamic Lagrangian code MULTI at $I=7.5\times10^{13}$ W cm^2 corresponding to a shock velocity of 32 km s^{-1}. The discontinuity corresponds to the denser PVCD layer. We note that, in this figure, x is the Lagrangian coordinate used in the computer program, and *not* the distance. It corresponds to the initial thickness of the uncompressed material, and then it does not change during the simulation. In real space, instead, any compression of the material would correspond to an equal reduction in target thickness.

was sandwiched between 26 μm of polyethylene (CH_2) on the side of the compression beams and 10–104 μm of polyethylene on the CPA side. Experimental data are shown in Fig. 1. No $K\alpha$ emission above noise was observed for 104-μm targets. Here, instead of showing averaged values as in Ref. [5], the individual experimental points are shown together with a typical error bar and the interpolation obtained by means of Harrach and Kidder's model [13]. According to this model, the relationship between the penetration depth (R_0) and the temperature of the fast electrons (T_{fast}) is $R_0=bT_{fast}^{1+\mu}$, while the energy deposition is proportional to $\exp(-\beta\sqrt{x/R_0})$, where x is the distance traveled inside the target in the direction perpendicular to the surface. Here the parameters b and μ are obtained by fitting Spencer's data [14] on the stopping power with a power law, while β takes also into account the Maxwellian distribution and the opening angle (90°) of the fast electron source. For the coefficients we have used $\beta=1.85$, $b=4.6\times10^{-6}$, and $\mu=0.78$ (with R_0 and T_{fast} measured in g cm^{-2} and keV, respectively), the values given for carbon. A calculation for plastic based on Bragg's additivity, that is, averaging Z on the mass of the components [15], yields almost identical values (the stopping power of CH_2 is mainly due to carbon). This allows us to define a penetration depth and to evaluate the temperature of fast electrons from the penetration depth in cold matter. For the uncompressed targets we obtain $R_0=3.7\pm1.0$ mg cm^{-2} (distance times target density), equivalent to 39 μm of pure CH_2 ($\rho=0.94$ g/cm^3). This gives a fast electron temperature of order 43 keV, in sufficient agreement with the scaling law found by Beg *et al.* [11], from experiments on the same laser system,

$$kT_{fast}=100(I_{17})^{1/3}\ \text{keV}, \tag{1}$$

where I_{17} is intensity in units of 10^{17} W cm^{-2}, which gives 46–84 keV for intensities $(1-6)\times10^{16}$ W cm^{-2}. We also used CR39 plastic ion-track detectors, which, calibrated according to Ref. [11], yielded temperature values between 30 and 57 keV, depending on laser intensity.

In compressed targets a penetration depth of 7.2 ± 2.0 mg cm^{-2} was found, equivalent to 77 μm of, original, uncompressed CH_2, an increase of almost 100% (in compressed matter the actual thickness is only 24 μm). The total stopping power of the target has been halved by compression, a very surprising result. We were careful to ensure that the conditions of the CPA interaction were identical in each case, the CPA beam was fired before shock breakout and preheating was minimized. Hence this result cannot be due to a change in the fast electron temperature. The $I\lambda^2$ of the compression beams is too low for fast electron generation [16], and MULTI simulations show that the fluor layer is not heated sufficiently to cause $K\alpha$ emission, as was also verified experimentally by firing the ns beams alone. This was one of the goals of the 26-μm CH_2 layer, the other one being to avoid $K\alpha$ emission due to fast electrons going around the target [5]. The variation in $K\alpha$ cross section in the compressed material is negligible. Thus the increase must be due to a change in the electron transport.

In Sec. II we model the electron transport and $K\alpha$ emission with a purely collisional code, the normal method of interpretation for such experiments (e.g., Beg *et al.* [11]), paying particular attention to the changes in stopping power as the target is ionized. We show that there is, at most, a 25% reduction in the stopping power in compressed targets. In Sec. III we consider how electric field generation could account for this discrepancy, following the model recently developed by Bell *et al.* [17]; we will also see how the electric field and its induced deceleration act to produce an apparently lower temperature of the fast electrons. In Sec. IV we model the electron transport with a Fokker-Planck hybrid code, including both collisions and field generation. This shows that a reduction in energy loss to the electric field due to the compression can account for the observed penetration increase. Finally Sec. V gives the conclusions.

II. COLLISIONAL MODELING

We have written a code to model the $K\alpha$ emission following the approach already used in Ref. [11]. We use the stopping power formula developed by Val'chuk *et al.* [18], which was also used by Deutsch *et al.* [3] (note the printing error in the stopping power formulas in this paper, as verified with the authors);

$$\frac{dE}{dx}=-\frac{4\pi e^4}{E}[n_bL_b+n_f(L_f+L_w)], \tag{2}$$

where n_f is the free electron density, n_b is the bound electron density and L_b, L_f, and L_w are the stopping numbers for bound electrons, free electrons, and for the generation of plasma waves, respectively. We have neglected bremsstrahlung radiation, since this is only important for high Z materials and ultrarelativistic electrons. As the stopping power is proportional to the total electron density, the observed

change in penetration depth ($\mathrm{mg\,cm^{-2}}$) must be due to a change in the effective stopping number.

L_b is dominated by $\ln(4E/I_0)$, for the energies we are interested in, where E is the fast electron kinetic energy and I_0 is the mean excitation potential [15]. This is an average energy which takes into account the energy lost by fast electrons as a consequence of excitation and ionization of background atoms. Apart from relativistic terms, L_f is given by the Coulomb logarithm [$L_f = \ln(\lambda_D/2\lambda_{dB})$, where λ_D is the Debye length and λ_{dB} is the de Broglie wavelength of the fast electrons] [18,19]. L_w gives a relatively small increase to L_f [20,21]. It has been included for the sake of completeness. Strictly, it is only accurate for a single particle. For a group of fast electrons the energy gain from the absorption of plasma waves should also be included [21,22]; this effect can cause a rapid velocity scattering for a monoenergetic distribution, but for a Maxwellian it has no net effect [22,23].

The $K\alpha$ emission from the PVCD fluor is calculated using the K shell ionization cross section [24,23],

$$\sigma_K \ (\mathrm{cm^2}) = 7.92\times 10^{-14}\frac{1}{EE_K}\ln\frac{E}{E_K}, \tag{3}$$

where E_K is the K shell ionization energy (2822 eV for Cl) and energies are in eV, and the $K\alpha$ yield [25] (which takes into account the possible deexcitation by Auger electrons)

$$\omega_K = \frac{Z^4}{Z^4 + 1.12\times 10^6}, \tag{4}$$

where Z is the atomic number of the emitter ($Z=17$ for Cl). Finally, we consider the x-ray absorption due to the plastic between the emitting layer and the spectrometers using the absorption coefficients given by Ref. [26].

We treat the uncompressed targets as cold matter with $n_f = 0$, so only the first term contributes. For I_0 we use the values tabulated by the International Committee on Radiation Unit (ICRU) [15] (these values are more detailed, although similar, to those reported by Spencer [14]).

For the shock-compressed targets we use the results of the hydrocode MULTI for the target temperature and density and calculate the degree of ionization with the formulas given by More, based on the Thomas-Fermi atomic model [27]. This gave a mean ionization $Z^* = 1.7$. The mean excitation potential, for an ion of ionization state q I_q is calculated following More [28]:

$$I_q = I_0\frac{\exp(1.29(q/Z)^{0.72-0.18q/Z})}{\sqrt{1-q/Z}}. \tag{5}$$

Angular scattering is neglected and the electrons are assumed to propagate in straight lines. As only collisional effects are included and the target conditions are assumed constant the electron trajectories are independent. We assume an exponential energy distribution with temperature 43 keV, as calculated Sec. I. The use of such an exponential distribution law, i.e., $n(E) = n_0\exp(-E/T)$, arises from comparison with previous experimental works reported in literature [11,29] and above all with the results of particle-in-cell simulations [30]. Let us note explicitly that this is *not* a Maxwellian distribution, although many works erroneously refer to it in this way. Even if the two distributions have almost the same behavior at high electron energies, the parameter T in the exponential law is not, strictly speaking, the fast electron temperature but their average energy. Hence care must be taken when the results of different works are compared.

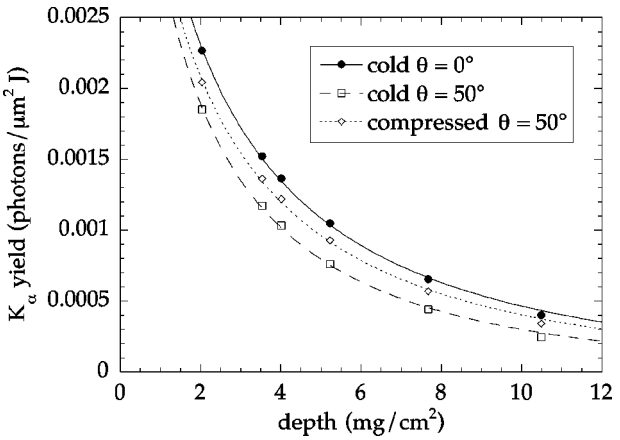

FIG. 3. $K\alpha$ yield and penetration depth for cold matter with $\theta = 0°$ (solid line, $R_0 = 4.7\ \mathrm{mg\,cm^{-2}}$), with $\theta = 50°$ (dashed line, $R_0 = 3.6\ \mathrm{mg\,cm^{-2}}$), and for compressed matter with $\theta = 50°$ (dotted line, $R_0 = 4.5\ \mathrm{mg\,cm^{-2}}$). Only stopping power effects, including the electron degeneracy, are taken into account.

Having chosen the distribution law, leaves us with two free parameters: the cone angle of emission and the total energy of the fast electrons. The cone half angle was varied to give the best fit to the experimental penetration range obtained from the points in Fig. 1. 50° gave a good fit for the uncompressed targets and approximately also for the compressed ones. The fact that the same angle reproduces both cases indicates that the increased propagation in compressed targets is not due to a decrease in angular scattering. Figure 3 shows the results of the $K\alpha$ yield for cold and compressed matter with $\theta = 50°$ (the result for $\theta = 0°$ in cold matter is shown for the sake of comparison). As angular scattering is neglected in the code, this angle represents not only the actual cone angle of emission but also the average angular scattering in the target. Thus, it is not in contradiction with the lower values obtained in other works, e.g., Ref. [31]. The root mean square angular scattering increases linearly with the penetration distance [32,33], and can be evaluated to be $\approx 40°$ at 40 μm. This implies a significantly lower initial cone angle ($\leqslant 30°$), assuming a quadratic sum. The energy into fast electrons was determined by matching the code results to the experimentally determined total number of emitted $K\alpha$ photons from the uncompressed targets. In order to do this, we took into account the collection solid angle, the film sensitivity [34], the absorption due to the beryllium filters [26] and the pentacrythritol (PET) crystal reflectivity [35]. This gave an absorption of 20% of the laser energy into fast electrons. This is in approximate agreement with other results on the absorption fraction [11,31,36].

The code gives a *maximum* increase in the penetration depth in compressed targets of 20%, compared to the almost 100% measured increase. This decrease in the total effective stopping number is largely due to the significant decrease in L_b [an increase in I_q, Eq. (5)] with ionization, as the remaining electrons are more tightly bound. Moreover, the stopping

power of an electron decreases when it leaves the atom ($L_f < L_b$ in our case), and L_f is also lower in compressed targets, due to the higher density, which lowers the Debye length and the mean interparticle separation. The relatively small change is not surprising, as the parameters which change appear in logarithmic terms. Also, at high enough electron energies, stopping numbers become material independent, depending only on the fast electron kinetic energy [15].

The effect of electron degeneracy is not included in Val'chuk *et al.*'s formulas. This will reduce L_f, as it has the effect of preventing energy losses to the free electrons of less than the Fermi energy, and L_b, since it produces an effective increase in the mean excitation potential to $\approx I_q + E_F$. Simply including such a cutoff for a Fermi energy of 22 eV (Sec. I) gave an increase in the penetration range of the order of 5%. Correlation is not expected to play a significant role as the de Broglie wavelength of fast electrons much smaller than the mean ion-ion distance in the compressed target, so that the incoming electrons only ''see'' one ion at a time. The density effect correction [15] has also been calculated to play a negligible role in our case. Also, as stated in Sec. I, we verified that the change in the $K\alpha$ yield as a result of compression is negligible.

However, there is a more important effect that has been neglected in the model: heating and ionization of the target by the fast electrons. To estimate the average fast electron heating in the uncompressed targets, we use a volume defined by a 100-μm spot diameter, a 36-μm penetration distance and 50° cone half angle, and 3 J of fast electron energy (20% of 15 J), and assume this energy heats every electron in this volume. This gives a temperature of $\sim 5-10$ eV, of the same order as the heating due to the compression of the targets. Given the greater penetration distance, the induced heating in compressed targets would be around half this. Thus to accurately calculate the change in the stopping power requires a self-consistent calculation, taking into account the heating and collisional ionization of the target by the fast electrons. This greatly complicates the calculation, making the electron trajectories no longer independent. However, we can see that this effect will reduce the difference in ionization between the uncompressed and compressed targets, reducing the difference in stopping power, which is already significantly lower than that observed in the experiments. So we can conclude that changes in the collisional stopping power, though not negligible as is often assumed, cannot explain the experimental results.

III. ELECTRIC FIELD EFFECTS

As the fast electrons enter the target they will set up an electric field which will act to slow them down and draw a return current of target electrons. This return current is essential to the propagation of the fast electrons, as otherwise they would be prevented from propagating by the electrostatic field setup. The return current requires an electric field to be maintained, dependent on the target conductivity, which will slow the fast electrons. We can immediately see that this is a more likely reason for the significant change in the penetration with compression, as energy loss to the electric field depends directly on the distance traveled (from $\int \mathbf{E} \cdot d\mathbf{l}$). The conductivity in the compressed targets is also expected to be higher. A number of authors have considered electric field effects [17,31,37,38]. Bell *et al.* [17] derived a mean penetration depth for fast electrons, from a one-dimensional (1D) model including only the electric field and assuming a constant conductivity, which provides a good starting point for assessing field effects

$$z_0 \approx 46 \left(\frac{T_{fast}}{43\ \text{keV}} \right)^2 \left(\frac{\sigma}{10^6\ \Omega^{-1}\text{m}^{-1}} \right) \left(\frac{0.2}{f_{abs}} \right) \times \left(\frac{6 \times 10^{16}\ \text{W cm}^{-2}}{I} \right) \mu\text{m}, \tag{6}$$

where σ is the target conductivity and f_{abs} is the absorption into fast electrons. We expect this to be an underestimate of the penetration depth as, being 1D, it does not include the fall in fast electron current density as the electrons spread out and, having a fixed conductivity, does not include the time variations of conductivity due to fast electron heating, which were shown to be significant in Sec. II.

In the literature several models are available for calculating the conductivity of materials [39–43], but all these are basically derived and valid for metals (or plasmas). Indeed they give a conductivity which is nonzero at room temperature. For insulators, such as plastic, the important factor is that changes in conductivity are mainly driven by changes in the effective ionization of the material, which is zero at room temperature. Hence we turned to a simpler classical model to estimate the minimum conductivity for the compressed targets from the MULTI results (Sec. I),

$$\sigma_{min} = \frac{n_c e^2 l}{v_c m_e}, \tag{7}$$

assuming the conduction electrons have a mean free path l equal to the mean interatomic spacing ($\sim n_{atom}^{-1/3}$) [40,44–47], a number density n_c given by the free electron density, and a mean speed v_c given by the thermal velocity. This gives $\sigma_{min} \sim 10^6\ \Omega^{-1}\,\text{m}^{-1}$ which is in fair agreement with the value given by the quantum–mechanical model by Kitamura and Ichimaru [39]. This value is quite high, being very close to the conductivity of Al at the same temperature (although at room temperature Al has a higher conductivity: $\sigma = 3.5 \times 10^7\ \Omega^{-1}\,\text{m}^{-1}$). Using the calculated values of T_{fast} and f_{abs} (Sec. I) and a maximum intensity of $6 \times 10^{16}\ \text{W cm}^{-2}$ gives us a lower estimate of the penetration depth $z_0 \approx 46\ \mu$m. Comparing this to the maximum, total, compressed target thickness of 50 μm, and the experimental penetration depth of $\approx 24\ \mu$m shows that electric field effects are not important in the compressed targets.

The same procedure can be used, in principle, to evaluate electric effects in uncompressed targets. However, the conductivity in the uncompressed targets is a more complex issue. For instance, the initial, cold, conductivity ($\sim 10^{-11}\ \Omega^{-1}\,\text{m}^{-1}$) gives effectively zero penetration, and electric fields orders of magnitude higher than the breakdown threshold (20 MV/m for our plastic [48]). This shows that the fast electrons cannot propagate in the uncompressed targets without first breaking down, or ionizing, the target. The above calculations indicate that a significant degree of ionization is required to give a z_0 comparable to the measured penetration depth. To estimate the energy required to turn the target into a good conductor, we use the same pro-

cedure used in Sec. II to estimate the heating of the target to calculate the energy required to singly ionize the carbon atoms (the lowest ionization energy), giving ~ 0.3 J. This is 10% of the fast electron energy for 20% absorption and 15-J laser energy. For the lower energy shots this could be quite a significant effect, though it may have a greater effect on the total yield than the penetration depth. A simple estimation of the average heating in uncompressed targets yielded a temperature of the same order of the compressed material, where the fast electrons are now the unique responsible for the heating (and hence the nonzero value of σ_{min}). All other factors being equal, a compression factor of 3.2 times would increase σ_{min} by a factor of $3.2^{2/3} \approx 2.2$, due to the factor of 3.2 increase in n_c and $3.2^{1/3}$ reduction in l. In the uncompressed targets, the conductivity, following breakdown, is then roughly half that of the compressed targets ($\sigma \approx 4.5 \times 10^5\ \Omega^{-1}\,\mathrm{m}^{-1}$). Hence z_0 will be decreased of a factor ≈ 2, while the target thickness is larger by a factor ≈ 3 in the uncompressed target. We stress the fact that, despite the uncertainties on the value of σ as derived from different models, the real important fact for our modelization is the change between the uncompressed and compressed cases. All models give a larger conductivity in the last case.

Thus we can conclude that the electric field is not important in the compressed targets, but will reduce the penetration in the uncompressed targets. To calculate its effect we require a much more detailed, 2D calculation, taking into account the fast electron heating of the target and collisions. Before we proceed to this in Sec. IV, there is another important conclusion to make from this; the purely collisional models we applied to the uncompressed target results in Secs. I and II and [5] to obtain the fast electron temperature and absorption are not valid, but they are valid for the compressed target results. So Harrach and Kidder's model should be applied to compressed matter. The higher penetration in the compressed targets gives a fast electron temperature of order 64 keV, instead of 43 keV (we used the same method of Harrach and Kidder to find ''revised'' values for the coefficients β, b, and μ on the basis of Val'chuk *et al.*'s stopping power for the compressed matter). This gives better agreement with Eq. (1), and is at the upper end of the temperatures indicated by the ion measurements (Sec. I). The higher $K\alpha$ yield indicates an absorption somewhat higher than the 20% calculated in Sec. I. This significantly changes the conclusions on the fast electron generation. This higher temperature would also further reduce the difference in stopping power between the cold and compressed targets calculated in Sec. II.

IV. FOKKER-PLANCK MODELING

To investigate all these effects, in a more detailed way, we used the Fokker-Planck hybrid code developed by Davies and co-workers [38,49,50], following the same basic setup used in these papers. The code represents the fast electrons with a relativistic Fokker-Planck equation, including drag [Eq. (2)] and angular scattering, which is solved using a particle, Monte Carlo method. The target is represented by $\mathbf{E} = \mathbf{j}_b/\sigma$, where $\mathbf{E}$ is the electric field and $\mathbf{j}_b$ is the background current density. The conductivity is a specified function of the background temperature, which is increased by fast electron collisional and Ohmic losses using a temperature-dependent heat capacity, obtained from the Thomas-Fermi model. To find the fields, Maxwell's equation are solved, neglecting the displacement current and assuming rotational symmetry, giving electric and magnetic fields $E_r(r,z)$, $E_z(r,z)$, and $B_\theta(r,z)$.

As an illustration, we considered the simplified problem of uniform CH_2 targets with average density 1.04 $\mathrm{g\,cm}^{-3}$, and a uniform compression factor of 3.2 in the compressed case. The different materials, uncompressed layers and preheated layers (due to the CPA prepulse) were not considered. Targets consisting of, before compression, 10-, 30-, 50-, 70-, and 100-μm layers followed by 13.5 μm of, nominal, fluor layer and then a further 26 μm, as in the experiment, were modeled. The relative $K\alpha$ yield was calculated from the total collisional energy loss of fast electrons in the nominal fluor layer, using the $K\alpha$ energy (2822 eV) instead of the mean excitation potential. Cold solid collision coefficients were used in both cases, to illustrate only the change in electric field effects.

A wide range of conductivities, electron temperatures, absorptions and angular distributions were used with open and reflective boundaries for the lowest and highest intensities used in the experiment (in total 32 sets of runs were performed). The main conclusions from these runs are the following.

(1) The magnetic field is not significant, due to the large spot radius.

(2) The electric field is not significant in the compressed targets.

(3) The electric field in the uncompressed targets lowered the penetration depth and $K\alpha$ yield.

Within the range of physically sensible parameters and the experimental uncertainties, the penetration depths can be made to agree with the experimental results. As the compressed target results were found to be independent of the fields, the penetration depth was only dependent on the temperature and the cone angle. So we used these runs to narrow down the possible combinations of these values. Varying the cone half angle between 0° and 90° indicated temperatures between about 60 and 100 keV. In line with previous results, we concentrated on half angles between 0° and 35°. The inferred temperature does not vary significantly within this range of angles. Small cone angles also gave much better agreement with the penetration depth in uncompressed targets, as a wider cone angle gives a lower current density, due both to the greater spread of the electrons and the lower background temperature it implies, and hence higher electric field. Of course, the conductivity in the uncompressed target can be lowered until the penetration depth agrees, but this gave unrealistic conductivities. We will now discuss one set of runs in detail, the basic procedure was the same for all runs.

For the conductivity we used the simple, heuristic model introduced in Refs. [49,50],

$$\sigma = \sigma_{min} + \sigma_{Spitzer}, \tag{8}$$

where σ_{min} is an initial, minimum, conductivity, estimated from Eq. (7) (Sec. III), and $\sigma_{Spitzer} = 10^4 (Z \ln \Lambda)^{-1} (kT)^{3/2}$

$\Omega^{-1}\,\mathrm{m}^{-1}$ is the Spitzer conductivity, with kT the temperature of the target in eV. $Z\ln\Lambda=8$ was used in both cases. For $\sigma_{Spitzer}$ to equal $10^6\ \Omega^{-1}\,\mathrm{m}^{-1}$ requires $T=22(Z\ln\Lambda)^{2/3}$ eV, indicating that the conductivity will not increase significantly above σ_{min} due to fast electron heating. The reason for proposing this equation is that mean free paths of the order of the interatomic spacing have been inferred in a number of different laser experiments [44–47], and at higher temperatures we expect to obtain the Spitzer value. It is also in line with estimates of the mean free paths taken from the theoretical work of Lee and More [40]. The value of σ_{min} is also restricted by physical limits on the maximum electric field that can be generated [49,50]. For the compressed targets we used $\sigma_{min}=10^6\,\Omega^{-1}\,\mathrm{m}^{-1}$, as calculated in Sec. III, and for the uncompressed target we used $\sigma_{min}=4.5\times10^5\ \Omega^{-1}\,\mathrm{m}^{-1}$, a factor of 2.2 lower; simulations in a wide range of σ do not show appreciable changes. An evaluation of Eqs. (7) and (8) using the SESAME equation of state to obtain the free electron density as a function of temperature indicates that this value may slightly be too high. However, one must also bear in mind that collisional ionization and electrical breakdown are likely to lead to a higher free electron density than in equilibrium. For the fast electron propagation not to be significantly inhibited by electrostatic fields there must be a background, free electron density much higher than the fast electron density. The initial electrical breakdown is ignored in the model, being assumed instantaneous.

The fast electron generation was calculated from an assumed laser intensity

$$I(r,t)=I_p e^{-r^2/R^2}e^{-4(t-t_p)^2/\tau^2} \tag{9}$$

with peak intensity $I_p=6\times10^{16}\ \mathrm{W\,cm}^{-2}$, spot radius $R=50\,\mu\mathrm{m}$, and pulse duration $\tau=3$ ps, and with the pulse peak at $t_p=3$ ps, which is just a computational parameter that determines at what point the fast electron generation is turned on. This gives a total laser energy of 12.5 J and an average intensity, calculated from the total energy delivered within the spot radius and pulse duration, of $2.8\times10^{16}\ \mathrm{W\,cm}^{-2}$. This corresponds to the higher energies and best focus achieved in the experiment. In this case the initial breakdown can be more reasonably neglected, as only a small fraction of the fast electron energy is required to ionize the target (Sec. III). An $e^{-E/kT}$ distribution was used, where E is the electron kinetic energy, and with the mean energy kT given by

$$kT(r,t)=143I_{17}^{1/3}(r,t)\ \ \mathrm{keV}. \tag{10}$$

This gives a mean electron energy (total electron energy divided by total number of electrons generated) of 66 keV, which agrees with the results obtained from Eq. (1) using the average intensity given above and with the higher temperature calculated, at the end of Sec. III, from the penetration depth in the compressed targets (again we stress that kT here is the mean electron energy, *not* the real temperature). The initial number density was calculated from

$$n_0(r,t)=\frac{f_{abs}I(r,t)}{v(r,t)kT(r,t)}, \tag{11}$$

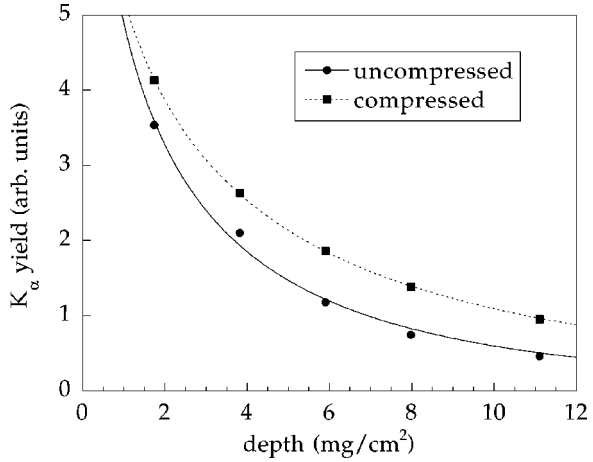

FIG. 4. Results from the Fokker-Planck modeling for an overall mean electron energy of 64 keV, an opening angle of 20° and reflective boundaries. Circles represent uncompressed targets ($R_0=3.61\pm0.35\ \mathrm{mg\,cm}^{-2}$), while squares represent compressed targets ($R_0=6.51\pm0.08\ \mathrm{mg\,cm}^{-2}$).

where v is the mean electron speed and absorption $f_{abs}=0.3$, a higher value than that calculated in Sec. II, to take account of the additional energy loss to the electric field. The electrons were fired into the target at a random angle, uniformly distributed in a cone of half angle 20°. This is lower than the value obtained in Sec. II, as angular scattering is included here. The electrons were specularly reflected at the boundaries.

The results for the relative $K\alpha$ yield are given in Fig. 4 together with fits using Harrach and Kidder's model. The penetration depths obtained from the fits are 3.61 ± 0.35 and $6.51\pm0.08\ \mathrm{mg\,cm}^{-2}$ for the uncompressed and compressed targets, respectively, which compare well with the experimental results of 3.7 ± 1.0 and $7.2\pm2.0\ \mathrm{mg\,cm}^{-2}$. The difference between the yields are not quite as large as those obtained in the experiment, particularly for the thinner targets. This was the case for all the runs performed, which matched the penetration depths well. This could be due to the initial energy loss in electrical breakdown. However, within the experimental uncertainties and the uncertainties in the model parameters, we cannot draw any definite conclusion on this.

Harrach and Kidder's collisional model always gave a better fit to the compressed target results than to the uncompressed ones. This is not entirely surprising, as the fields are not significant in this case, but they assumed a 90° half angle. The reason their model for the energy deposition still gives a good fit for sources with narrow cone angles is probably due to the angular scattering, which causes the electrons to rapidly ''forget'' their initial cone angle. Of course, the relation between the fast electron temperature and the penetration depth varies with cone angle, it is only the functional form of the energy deposition with depth that does not noticeably change. Thus we can conclude that electric field effects can readily account for the experimental results.

V. CONCLUSIONS

With hindsight, these shock compression experiments provided an excellent method of evaluating electric field

transport inhibition. The compression did not change the areal density, which is the major factor in the collisional stopping power, but did significantly reduce the thickness and, due to the higher electron density, significantly increased the minimum conductivity, factors which significantly affect losses to the electric field. In this case it put us in a regime where electric field effects were unimportant. Due to the large spot radius used, the magnetic field effects were also unimportant, whereas in most laser-solid experiments they are dominant [38,49–52]. Thus the only significant difference between the uncompressed and compressed targets is the electric field. The only change in the total collisional stopping power is in the argument of the logarithmic terms, which are relatively insensitive to the value of the argument, and, for the electron energies of interest, are dominated by the electron kinetic energy. In our case a maximum decrease of 25% in the collisional penetration depth in the compressed targets was found.

An important conclusion from this is that the traditional collisional analysis of the results should have been carried out on the compressed target results, rather than the uncompressed results. This indicates a fast electron temperature of around 64 keV and an absorption of about 30%, instead of 43 keV and 20% obtained from the uncompressed data. The fast electron source is the same in both cases, as in both cases they were generated by interaction with the same uncompressed material, it is just that the electric field slows the electrons in the uncompressed targets. With the inclusion of electric field effects the electron trajectories are no longer independent, and the penetration depth becomes dependent on the absorption, target conductivity, and heat capacity. The results in the uncompressed targets were found to be consistent with modeling using a Fokker-Planck hybrid code, which included all these factors. However, it is difficult to draw precise conclusions from these results due to the uncertainty in the parameters involved. The interpretation of the compressed target results is much more straightforward, giving the best way of determining the fast electron temperature and cone angle. Though the temperature inferred varies between 60 and 100 keV, increasing with the cone angle, the higher cone angles did not give agreement with the uncompressed target results in the Fokker-Planck modeling. Thus we can state that the fast electron temperature is around 64 keV, with a good degree of confidence.

It is interesting to note that the higher temperature obtained from the compressed targets is in better agreement with the temperature scaling given in Eq. (1), which was obtained from purely collisional modeling of similar experiments [11]. However, they used conducting targets. The results from the Fokker-Planck hybrid code given in Ref. [38] for aluminum targets, for laser parameters similar to those used in Ref. [11], indicated that the error in a purely collisional model would largely be in the absorption, rather than the temperature. This is because the energy deposition as a function of depth into the target has a similar gradient with and without fields included [38]. Beg *et al.* [11] used higher Z metals than aluminum, which would further increase the importance of the collisional terms. This higher temperature is greater than the temperatures inferred from the ion emission. However the ion measurements, being a more indirect method, are prone to a high degree of uncertainty, thus we do not believe that this difference is significant. Also, it should be noted that ion emission measurements are not an independent measure of the fast electron temperature, as the relation between ion energy and fast electron temperature was established by comparing experimental results on ion emission with results on fast electron temperature. Thus they are equally prone to errors from the neglect of field effects. In general, field effects must be considered in the interpretation of electron transport experiments. The main value of the compressed target results is that field effects can be discounted. The uncompressed results then give an excellent example of the effect of electric fields and the errors that can occur in neglecting field effects.

Another important conclusion from our work is that the fast electron heating and ionization of the target has a significant effect on their transport. In insulators the fast electrons induce a rapid phase transition from insulator to conductor. Thus the differences between insulators and conductors will be nowhere near as large as the differences between their cold conductivities would indicate. The major difference will come in the initial phases, when the conductivity of metals falls with increasing temperature and insulators must be broken down, in order for the electrons to be able to propagate. The fast electron energy per area will be the significant factor in this, as for a given penetration depth it determines the extent to which the fast electrons can heat the target. It appears to be largely because this is relatively low in these experiments that the effect of the electric field is so pronounced, even at intensities as low as 10^{16} W cm^{-2}. For the lower energy shots, included in the experimental results, the energy required to break down the target is a significant fraction of the fast electron energy, further complicating the interpretation.

Computer simulations also allow a separate evaluation of collisional heating due to fast electrons and Joule heating due to the return current of background electrons. Most of the energy loss is collisional, and for the compressed target it is entirely collisional, since electric field effects are negligible. For uncompressed runs up to 18% of the total energy is lost to the electric field: it varies with target thickness, as the electrons reflected from the rear surface of the thinner targets lower the total fast electron current. For the thinnest targets it was 14%. The effect of the fast electron heating on the collision coefficients is also not negligible, although the up to 25% decrease in the collisional stopping power found in Sec. II was largely due to the ionization, and a high degree of ionization in the uncompressed targets is caused by the fast electrons.

Thus our final answer is that the almost 100% increase in fast electron penetration in compressed matter [5] is due, almost entirely, to the reduction in energy loss to the electric field, due to the reduction in the distance the fast electrons have to travel against the electric field and to the higher conductivity, lowering the field. The alternative is that there are no electric field effects and there is a dramatic reduction in collisional stopping power in the compressed material, which cannot be explained by any current theory. These results represent the first clear demonstration of the effect of electric field in $K\alpha$ electron transport experiments. It confirms the suggestion of previous theoretical works [17,37,38] that purely collisional models will underestimate the tem-

perature and absorption into fast electrons. The compressed target results allow a clear evaluation of the fast electron temperature, free of the complex considerations of field generation. In particular we found that, at intensities of a few 10^{16} W cm^{-2}, 25–30 % of the laser energy is absorbed into fast electrons with a temperature of approximately 64 keV, entering the target in a relatively narrow cone half angle ($\approx 30°$). Recent important experiments by Key and Wharton *et al.* [31], measured fast electron generation and propagation at laser intensities up to 10^{19} W cm^{-2}. Some of their results have also been interpreted as being, in part, due to electric field effects. However, in this experiment the laser was fired on different materials, changing at the same time the characteristics of the hot electron source and the propagation in the medium. In particular, the authors obtained results in plastic and in metals, but a comparison is not straightforward, since both the collisional and the electric properties of the materials changed simultaneously. Indeed the authors themselves only considered as ''tentative'' an explanation based on electric field effects. In our case we use the same material and the same areal density and, practically, the only important change between the compressed and the uncompressed case is in the electrical properties of the medium. Also, in Key and Wharton *et al.*'s experiments magnetic fields play an important role, which is not our case. Hence we conclude that our result represent a much clearer, direct, and sure proof of the importance of electric fields effects.

We stress that, even though the laser intensity used in the experiment is lower than those intensities required for fast ignition, nevertheless the results are of direct interest for such a scheme. Indeed due to the quite weak scaling of fast electron temperature with laser intensity, even at 10^{19} W cm^{-2} we could obtain $\gtrsim$400-keV electrons. Now the propagation of such electrons in matter is not so different from the propagation of 60-keV electrons. In both cases we have fast electrons which propagate in a strongly correlated, degenerate material which is characterized by a typical parameter I_0 much lower than the electron energy. Of course experiments performed at higher intensities are desirable, but it must be considered that increasing the electron energy will increase the penetration range, which implies the use of thicker targets which cannot be uniformly compressed with the available laser beams. Hence, at least considering the compression aspect, a less clean experiment would be realized, which is not, we think, what is needed for fast ignition studies in this phase. The other critical point is of course how to increase compression, our values still being very far from those desired for fast ignition.

Finally, we reemphasize that to our knowledge these experiments represent the first experimental results on the propagation of fast electrons in compressed matter, results which this paper has been able to greatly clarify. The compressed targets provide a more than three times solid density, degenerate plasma. This is of interest to the fast ignitor scheme, and in all fields in which electron propagation in degenerate matter can play a role, e.g., dense stellar surfaces and the cores of giant planets.

ACKNOWLEDGEMENTS

This work was supported by the European Union TMR programmes ''Access to Large Scale Facilities'' (Contract No. ERBFMGEC950053), the Marie Curie Research Fellowships scheme (Contract No. ERBFMBICT983502), by the LEA ''High Power Laser Science,'' by the UK EPSRC (Grant No. GR/K19198) and by the European Science Foundation in the framework of the PESC program ''FEMTO.'' We also acknowledge the contribution of the Italian MURST under the research program ''Interaction of plasmas with nanosecond and picosecond lasers.'' The authors acknowledge useful discussions with M. Basko, C. Deutsch, J. C. Gauthier, M. Key, M. Lontano, J. Meyer-ter-Vehn, R. Sigel, and S. Wilks.

[1] M. Tabak *et al.*, Phys. Plasmas **1**, 1626 (1994).
[2] S. Atzeni, Jpn. J. Appl. Phys. **34**, 1980 (1995).
[3] C. Deutsch, H. Furukawa, K. Mima, M. Murakami, and K. Nishihara, Phys. Rev. Lett. **77**, 2483 (1996).
[4] D. Batani, A. Bernardinello, V. Masella, F. Pisani, M. Koenig, J. Krishnan, A. Benuzzi, S. Ellwi, T. Hall, P. Norreys, A. Djaoui, D. Neely, S. Rose, P. Fews, and M. Key, in *Superstrong Fields in Plasmas*, edited by M. Lontano, G. Mourou, F. Pegoraro, and E. Sindoni, AIP Conf. Proc. No. 426, (AIP, New York, 1998), p. 372.
[5] T. A. Hall, S. Ellwi, D. Batani, A. Bernardinello, V. Masella, M. Koenig, A. Benuzzi, J. Krishnan, F. Pisani, A. Djaoui, P. Norreys, D. Neely, S. Rose, M. H. Key, and P. Fews, Phys. Rev. Lett. **81**, 1003 (1998).
[6] C. Danson *et al.*, Opt. Commun. **103**, 392 (1993).
[7] M. Koenig, B. Faral, J. M. Boudenne, D. Batani, S. Bossi, and A. Benuzzi, Phys. Rev. E **50**, R3314 (1994).
[8] R. Ramis, R. Schmalz, and J. Meyer-ter-Vehn, Comput. Phys. Commun. **49**, 475 (1988).
[9] SESAME, The LANL equation of state database, LA-UR-923407 (1992).
[10] See, for instance M. Alonso and E. J. Finn, *Fundamental University Physics: Quantum and Statistical Physics* (Addison-Wesley, Reading, MA, 1968).
[11] F. N. Beg, A. R. Bell, A. E. Dangor, C. N. Danson, A. P. Fews, M. E. Glinsky, B. A. Hammel, P. Lee, P. A. Norreys, and M. Tatarakis, Phys. Plasmas **4**, 447 (1996).
[12] M. Schnurer, M. P. Kalashnikov, P. V. Nickles, Th. Schlegel, W. Sandner, N. Demchenko, R. Nolte, and P. Ambrosi, Phys. Plasmas **2**, 3106 (1995).
[13] R. J. Harrach and R. E. Kidder, Phys. Rev. A **23**, 887 (1981).
[14] *Energy Dissipation by Fast Electrons*, edited by L. V. Spencer, Natl. Bur. Stand. U.S. Monograph No. 1 (U.S. GPO, Washington, DC, 1959).
[15] International Committee on Radiation Units Report No. 37, I.C.R.U. (1984).
[16] S. J. Gitomer *et al.*, Phys. Fluids **29**, 2679 (1986).
[17] A. R. Bell, J. R. Davies, S. Guerin, and H. Ruhl, Plasma Phys. Controlled Fusion **39**, 653 (1997).
[18] V. V. Val'chuk, N. B. Volkov, and A. P. Yalovets, Plasma Phys. Rep. **21**, 159 (1995).
[19] *NRL Plasma Formulary*, edited by D. L. Book (Naval Re-

search Laboratory, Washington, DC, 1987).
[20] D. Pines and D. Bohm, Phys. Rev. **85**, 338 (1952).
[21] N. Rostoker and M. N. Rosembluth, Phys. Fluids **3**, 1 (1960).
[22] M. V. Nezlin, *Physics of Intense Beams in Plasmas* (Institute of Physics, London, 1993).
[23] L. D. Landau and E. M. Lifsits, *Kvantoaja Mechanika* (Mir, Moscow, 1976).
[24] M. Green and V. Cosslet, Proc. Phys. Soc. London **78**, 1206 (1961).
[25] G. Wentzel, Z. Phys. **43**, 524 (1927).
[26] B. L. Henke *et al.*, At. Data Nucl. Data Tables **27**, 1 (1982).
[27] R. M. More, in *Handbook of Plasma Physics*, edited by A. Rubenchik and S. Witkowski (North-Holland, Amsterdam, 1991), Vol. 3.
[28] R. M. More, in *Proceedings of the 29th St. Andrews Scottish Universities Summer School in Physics* (SUSSP Publications, Edinburgh, 1985), pp. 157–214.
[29] G. Malka and J. L. Miquel, Phys. Rev. Lett. **77**, 75 (1996).
[30] A. Pukhov and J. Meyer-ter-Vehn, Phys. Rev. Lett. **76**, 3975 (1996); **79**, 2686 (1997).
[31] M. H. Key *et al.*, Phys. Plasmas **5**, 1966 (1998); K. B. Wharton, S. P. Hatchett, S. C. Wilks, M. H. Key, J. D. Moody, V. Yanovsky, A. A. Offenberger, B. A. Hammel, M. D. Perry, and C. Joshi, Phys. Rev. Lett. **81**, 822 (1998); K. B. Wharton *et al.*, ICF Quart. Rep. **8**, 28 (1997).
[32] J. D. Jackson, *Classical Electrodynamics* (Wiley, New York, 1975).
[33] H. H. Hubbell, Jr. and R. D. Birkhoff, Phys. Rev. A **26**, 2460 (1982).
[34] P. D. Rockett, *et al.*, Appl. Opt. **24**, 16 (1985).
[35] N. G. Alexandropoulus and G. G. Cohen, Appl. Spectrosc. **28**, 2 (1974).
[36] S. Bastiani, P. Audebert, J. P. Geindre, Th. Schlegel, J. C. Gauthier, C. Quoix, G. Hamoniaux, G. Grillon, and A. Antonetti, Phys. Rev. E **60**, 3439 (1999).
[37] M. E. Glinsky, Phys. Plasmas **2**, 2796 (1995).
[38] J. R. Davies, A. R. Bell, M. G. Haines, and S. M. Guerin, Phys. Rev. E **56**, 7193 (1997).
[39] H. Kitamura and S. Ichimaru, Phys. Rev. E **51**, 6004 (1995).
[40] Y. T. Lee and R. M. More, Phys. Fluids **27**, 1273 (1984).
[41] M. W. C. Dharma-wardana and F. Perrot, Phys. Rev. E **58**, 3705 (1998).
[42] G. A. Rinker, Phys. Rev. B **31**, 4207 (1985).
[43] A. Benuzzi, M. Koenig, B. Faral, J. Krishnan, F. Pisani, D. Batani, S. Bossi, D. Beretta, T. Hall, S. Ellwi, S. Hüller, J. Honrubia, and N. Grandjouan, Phys. Plasmas **5**, 2410 (1998).
[44] H. M. Milchberg, R. R. Freeman, S. C. Davey, and R. M. More, Phys. Rev. Lett. **61**, 2364 (1988).
[45] B. T. Vu, O. L. Landen, and A. Szoke, Phys. Plasmas **2**, 476 (1995).
[46] A. Saemann and K. Eidmann, in *Superstrong Fields in Plasmas* (Ref. [4]), p. 270.
[47] P. M. Celliers *et al.*, Science **281**, 1178 (1998).
[48] Goodfellow Catalogue 1998/1999, Cambridge Science Park, Cambridge CB4 4DJ, England.
[49] J. R. Davies, A. R. Bell, and M. Tatarakis, Phys. Rev. E **59**, 6032 (1999).
[50] M. Borghesi, A. J. MacKinnon, L. Barringer, R. Gaillard, L. A. Gizzi, C. Meyer, O. Willi, A. Pukhov, and J. Meyer-ter-Vehn, Phys. Rev. Lett. **78**, 879 (1997).
[51] M. Tatarakis, J. R. Davies, P. Lee, P. A. Norreys, N. G. Kassapakis, F. N. Beg, A. R. Bell, M. G. Haines, and A. E. Dangor, Phys. Rev. Lett. **81**, 999 (1998).
[52] L. Gremillet *et al.*, Phys. Rev. Lett. **83**, 5015 (1999); F. Pisani *et al.* (unpublished).